Proceedings of ASME 2010 3rd Joint US-European Fluids Engineering Summer Meeting and 8th International Conference on Nanochannels, Microchannels, and Minichannels
FEDSM2010-ICNMM2010
August 2-4, 2010, Montreal, Canada

FEDSM-ICNMM2010-30171

PREDICTION AND MEASUREMENT OF THERMAL TRANSPORT ACROSS INTERFACES BETWEEN ISOTROPIC SOLIDS AND GRAPHITIC MATERIALS

Pamela M. Norris
Dept. of Mech. and Aero. Engr.
University of Virginia
Charlottesville, Virginia 22904
Email: pamela@virginia.edu

Justin L. Smoyer
Dept. of Mech. and Aero. Engr.
University of Virginia
Charlottesville, Virginia 22904
Email: jls5ra@virginia.edu

John C. Duda
Dept. of Mech. and Aero. Engr.
University of Virginia
Charlottesville, Virginia 22904
Email: duda@virginia.edu

Patrick E. Hopkins
Engineering Sciences Center
Sandia National Laboratories
Albuquerque, NM 87185
Email: pehopki@sandia.gov

ABSTRACT

Due to the high intrinsic thermal conductivity of carbon allotropes, there have been many attempts to incorporate such structures into existing thermal abatement technologies. In particular, carbon nanotubes (CNTs) and graphitic materials (i.e., graphite and graphene flakes or stacks) have garnered much interest due to the combination of both their thermal and mechanical properties. However, the introduction of these carbon-based nanostructures into thermal abatement technologies greatly increases the number of interfaces per unit length within the resulting composite systems. Consequently, thermal transport in these systems is governed as much by the interfaces between the constituent materials as it is by the materials themselves. This paper reports the behavior of phononic thermal transport across interfaces between isotropic thin films and graphite substrates. Elastic and inelastic diffusive transport models are formulated to aid in the prediction of conductance at a metal-graphite interface. The temperature dependence of the thermal conductance at Au-graphite interfaces is measured via transient thermoreflectance from 78 to 400 K. It is found that different substrate surface preparations prior to thin film deposition have a significant effect on the conductance of the interface between film and substrate.

NOMENCLATURE

D density of states, unitless
f_0 equilibrium distribution, unitless
h_{BD} thermal boundary conductance, [W m^{-2} K^{-1}]
$\hbar$ Planck's Constant, [J s]]
k wavevector, [m^{-1}]
k_{B} Boltzmann's Constant, [J K^{-1}]
q applied heat flux across the interface, [W m^{-2}]
T temperature, [K]
v phonon group velocity, [m s^{-1}]
ω phonon angular frequency, [rad s^{-1}]
ζ transmission coefficient, unitless

INTRODUCTION

Allotropes of carbon often exhibit extreme material properties due to the strong covalent bonds between atoms. In particular, carbon nanotubes (CNTs) and graphitic materials (i.e., graphite and graphene flakes, stacks, and nanoribbons) have garnered much interest due to the combination of both their thermal and mechanical properties [1]. In most cases, these materials are known for their strong anisotropy. For example, while they are axially stiff, they are laterally compliant. In turn, there have been many attempts to incorporate such nanostructures into existing thermal abatement technologies. Carbon nanotubes have been suspended in liquids to increase the overall effective thermal conductivity of the liquids [2, 3], as well as grown in arrays to act as thermal interface materials (TIMs) [4–7]. In addition, graphite has been implemented to structurally reinforce metallic heat spreaders while simultaneously increasing effective thermal conductivity [8, 9]. However, despite the fact that the intrinsic thermal conductivity, of these allotropes can exceed several thousand $\mathrm{W\,m^{-1}\,K^{-1}}$, their incorporation into existing abatement technologies does not always produce correspondingly impressive results.

An important concept to keep in mind when considering the effective phononic thermal conductivity of a nanostructured composite system is the phonon mean free path (MFP). The phonon MFP describes the average distance a phonon travels before it scatters. The number of scattering events phonons undergo as they travel through a medium is one of several factors that dictate thermal conductivity of the medium itself. A larger MFP leads to a higher thermal conductivity. To put this in context, the phonon MFP is on the order of 100 nm at room temperature in solids [10] but can vary over several orders of magnitude depending on the phonon frequency and the particular material in question [11]. In many nanocomposites, the interfaces between different materials, which act as additional scattering sites, are spaced at distances less than the phonon MFP. In turn, the presence of many closely spaced interfaces can reduce the effective phononic thermal conductivity of the composite system. Consequently, thermal conductivity is governed as much by the interfaces between the constituent materials as it is by the materials themselves. If we are to maximize the effective thermal conductivity of a nanostructured composite employing CNTs or graphitic materials, we must first better understand phonon transport across the interfaces within the composite. In the subsequent discussion, our primary focus will be on the interface between isotropic thin films and a graphite substrate.

The efficiency of phononic thermal transport across an interface is often described by thermal boundary conductance, h_{BD}, in units of $\mathrm{W\,m^{-2}\,K^{-1}}$. Thermal boundary conductance is generally a function of two factors: i) the vibrational (phononic) spectra of the materials comprising the interface [12] and ii) the condition of the interface itself [13].

With regard to the first factor, it would then be reasonable to assume that h_{BD} at a solid-graphite interface is affected by the combination of the reduced dimensionality and anisotropy of graphite [14], as well as the large vibrational mismatch between the film and graphite [12, 15]. For example, this vibrational mismatch is clear when looking at the phonon dispersion or density of states curves of metals and graphite. The maximum vibrational frequencies in metals are typically less than 10 THz [16, 17], whereas the maximum vibrational frequency in graphite is in excess of 45 THz [18]. This large vibrational mismatch opens up the possibility of inelastic phonon-phonon processes contributing to phonon thermal transport across solid-graphite interfaces [19, 20].

With regard to the second factor, the interfacial chemistry between metal films and graphite will have a significant impact on the reported value of h_{BD}. Metal-graphite interaction is often characterized by poor adhesion if significant carbide formation is not present. The poor adhesion at the metal-carbon interface is likely due to the fact that the stiff sp^2 bonds within a monolayer of graphite (graphene) prohibit significant chemical bonding between carbon and contacting materials, with interactions between the two instead described by weak dispersion forces. This theory has been experimentally demonstrated for Al [21] and Ti [22] on graphite. Additionally, it is well known that the adhesion energy at metal-graphite interfaces is fairly low ($\leq 500\ \mathrm{mJ/m^2}$) [23]. Weak dispersion forces are associated with low-frequency, low-energy vibrational modes. It is easy, then, to imagine this poor bonding will lead to poor thermal conductance across a solid-graphite interface.

To demonstrate the effect of poor adhesion on phononic thermal transport across interfaces, Prasher [24] developed the van der Waals Acoustic Mismatch Model. In this presentation, it was shown that low adhesion energies produce a significant reduction in interfacial thermal conductance. For example, the model predicts an 80% reduction in interfacial conductance when reducing the adhesion energy from 500 $\mathrm{mJ/m^2}$ to 100 $\mathrm{mJ/m^2}$. Molecular dynamics simulations have also been implemented to demonstrate that the lack of bonding between carbon allotropes and contacting materials will result in poor interfacial thermal conductance. Shenogin *et al.* [25] demonstrated that CNTs in octane liquid exhibit small thermal conductance at the CNT-liquid interface associated with the weak coupling between the rigid tube and the soft liquid (a similar situation to that of CNTs or graphene flakes embedded in polymer-based TIMs). Hu *et al.* [26] calculated that a single covalent bond between a CNT and a contacting Si surface would increase the interfacial thermal conductance by two orders of magnitude. Huxtable *et al.* [27] experimentally quantified h_{BD} at a CNT-liquid interface $\approx 12\,\mathrm{MW\,m^{-2}\,K^{-1}}$.

In the present work, we present extensions of the diffuse mismatch model (DMM) [28, 29] which can be implemented for the prediction of h_{BD} at solid-graphite interfaces. These models are improvements over the Diffuse Mismatch Model pre-

sented by Swartz and Pohl [30], as they account for both the anisotropy of graphite, as well as the possibility of inelastic scattering processes contributing to interfacial phononic thermal transport. However, these models do not take into account the bonding, or lack thereof, between metal films and graphite substrates. To experimentally assess the role of interfacial chemistry and bonding on thermal transport at solid-graphite interfaces, different surface preparations are used before thin Au films are deposited on graphite substrates. Thermal boundary conductance at these interfaces is measured via the transient thermoreflectance (TTR) technique from 78 to 400 K. This temperature dependent data is compared to modeled predictions, and the deviations from the models are discussed.

MODELING THERMAL BOUNDARY CONDUCTANCE

Two primary models have been most widely employed for predicting h_{BD} at interfaces between different materials: the acoustic mismatch model (AMM) and the diffuse mismatch model (DMM). The AMM treats phonons as waves propagating in a continuous medium and assumes these waves do not scatter at an interface between two different materials; rather, phonon transmission and reflection is controlled by the relative mismatch in acoustic impedance of the materials [31]. Due to this continuum analysis, the AMM works best at low temperatures where dominant phonon wavelengths are long and frequencies are low. The DMM, on the other hand, operates at the other extreme, assuming *all* phonons scatter at the interface and do so diffusely. That is, phonons lose memory of their incident polarization and direction after scattering at the interface [30]. As a result, the DMM holds for elevated temperatures relative to the AMM. Still, the overall accuracy of the DMM has more recently come into question as the model has been applied to a larger data set. Several studies [12, 32] have shown that the agreement between the DMM and experimentally measured values of h_{BD} can vary by up to an order of magnitude.

Derivation of the Diffuse Mismatch Model

The DMM has been derived in full several times in the literature [30, 33–37]. However, due to the varying assumptions applied during these derivations, many subtleties of the model are confused or even lost altogether [36]. As a result, the authors believe it is important to once again carry out this derivation. Not only will this ensure that these subtleties are not overlooked, but it will become possible to address the relative importance of these subtleties under the present set of assumptions. This being said, the phonon flux, q, across an interface from side 1 to side 2 can be represented as

$$q_z^{1\to2} = \frac{1}{(2\pi)^3}\sum_j \int_0^{\frac{\pi}{2}}\int_0^{2\pi}\int_{k_{x,1}}\int_{k_{y,1}}\int_{k_{z,1}>0} \hbar\omega_{j,1}(k_{j,1})\zeta^{1\to2} \\ |v_{j,1}(k_{j,1})| f_0 \sin(\theta_1)\cos(\theta_1) dk_{z,1} dk_{y,1} dk_{x,1} d\theta_1 d\phi_1, \quad (1)$$

where z is the direction of transport, j is the polarization, θ_1 and ϕ_1 are the azimuthal and elevation angles of the flux on side 1 approaching side 2 relative to the direction of transport, ζ is the transmission coefficient, v_1 is the carrier group velocity on side 1, f_0 is the equilibrium distribution of particles on side 1, and k is the wavevector. In order to consider only flux approaching the interface, integration is performed over half of the Brillouin zone and the absolute value of the group velocity, v_1, is taken. In this present study, the quantity of interest is phonon energy, and thus, the equilibrium distribution, f_0, is given by the Bose-Einstein distribution, $f_0 = 1/(\exp(\hbar\omega(k)/k_{\mathrm{B}}T) - 1)$. Assuming diffuse scattering, the directional dependance of Eq. 1 collapses and the expression for phonon flux across the interface from side 1 to side 2 becomes

$$q_z^{1\to2} = \frac{1}{8\pi^2}\sum_j \int_{k_{x,j,1}}\int_{k_{y,j,1}}\int_{k_{z,j,1}>0} \hbar\omega_{j,1}(k_{j,1})\,\zeta^{1\to2} \\ |v_{j,1}(k_{j,1})|\, f_0\, dk_{z,j,1}\, dk_{y,j,1}\, dk_{x,j,1}. \quad (2)$$

This expression can be further simplified by assuming the materials in question can be described by an isotropic phonon dispersion. This yields

$$q_z^{1\to2} = \frac{1}{8\pi^2}\sum_j \int_{k_{j,1}>0} \hbar\omega_{j,1}(k_{j,1})\, k_{j,1}^2\, \zeta^{1\to2}\, |v_{j,1}(k_{j,1})|\, f_0\, dk_{j,1}. \quad (3)$$

Under the diffuse assumption, the phonon transmissibility from side 1 to side 2 must relate to the phonon transmissibility from side 2 to side 1 via the expression $\zeta^{2\to1} = (1 - \zeta^{1\to2})$. Hence, through the application of detailed balance, $q_z^{1\to2} = q_z^{2\to1}$, it is possible to solve for $\zeta^{1\to2}$ explicitly. However, the formulation of the transmission coefficient is largely dependent on the assumptions invoked when applying detailed balance [36]. The transmission coefficient will be given explicit attention and specifically formulated for a metal-graphite interface in the next section.

The relationship between the phonon flux traversing an interface from side 1 to side 2 and h_{BD} can be established through a modified form of Fourier's law and noting that

$$q_z^{1\to2} = h_{\mathrm{BD}}^{1\to2} T^{1\to2} \Rightarrow h_{\mathrm{BD}}^{1\to2} = \frac{\partial q_z^{1\to2}}{\partial T^{1\to2}}, \quad (4)$$

where $T^{1\to2}$ is the temperature drop across the interface. It is important to note that, in the purely diffusive regime, the phonon transmission probability is predicted as 50% in the limit of the same material on either side of the interface. Although this has previously been ascribed to an incorrect physical limit [10], this is in fact a correct description assuming the most rigorous definition of diffusive scattering of particles (a scattering particle at a diffuse interface has equal probability of scattering in all available directions) [38]. That is, given an interface between two identical materials and assuming that phonons scattering at a perhaps imaginary interface will scatter diffusively, then phonons will have an equal probably of scattering in all directions (forward and backward) and therefore the transmission probably of the incident phonon flux will be 50%. With this in mind, h_{BD} is given by

$$h_{\mathrm{BD}}^{1\to2} = \frac{1}{8\pi^2}\sum_j \int_{k_{j,1}} \hbar\omega_{j,1}(k_{j,1})\, k_{j,1}^2\, \zeta^{1\to2}\, |v_{j,1}(k_{j,1})| \frac{\partial f_0}{\partial T}\, dk_{j,1}. \tag{5}$$

It is important to remember that, for all intents and purposes, the transmission coefficient has already been formulated at this point in the derivation of the DMM. As a result, it is critical that any restrictions or allowances regarding the range of participating phonons established during the application of detailed balance and the formulation of the transmission coefficient must be upheld here as well.

Application to Solid-Graphite Interfaces

When considering transport across a metal-graphite interface it is important to recognize the extreme anisotropy of graphite. This extreme anisotropy results in very complicated phonon dispersion relationships and is evident when examining the thermal conductivity, where *a*-axis (in the basal plane) and *c*-axis (perpendicular to the basal plane) values differ by three to four orders of magnitude [39, 40]. In addition to the anisotropy of graphite, the large difference in phonon cutoff frequencies, or vibrational mismatch, between most metals and graphite suggests that inelastic phonon scattering may provide an additional channel of energy transport across a metal-graphite interface [15, 19, 41]. Recently, a model was developed by Duda *et al.* [29] that accounts for inelastic scattering at interfaces where one material comprising the interface is characterized by high elastic anisotropy, such as graphite. Inelastic scattering is taken into account through a higher-harmonic approach outlined by Hopkins [42] and makes use of simplifying assumptions which are valid at elevated temperatures relative to the saturation temperature of vibrational modes in one direction.

Despite the complicated nature of the phonon dispersion relationships of graphite, an effective Debye density of states can be used to describe bulk graphite at temperatures above cryogenic [28, 40]. This is made possible by the weak interlayer vibration coupling in graphite, which can be described as a van der Waals type interaction and is associated with low-frequency vibrations. Dispersion diagrams of graphite show that acoustic interlayer vibrations exist at frequencies below 3 THz, 1 to 2 orders of magnitude below the longitudinal and transverse cutoff frequencies within the basal plane [18]. Additionally, studies examining both CNTs and graphite have indicated that interlayer acoustic modes saturate at temperatures above 50 K [14, 43].

Developing the effective density of states for predictions of h_{BD}, one can consider first a single monolayer of graphite, described by a two-dimensional Debye density of states. Scaling this density of states by N, or the number of two-dimensional subsystems per unit length, generates an effective density of states for the graphite system. The density of states for bulk graphite (or, likewise, multi-layer graphene stacks) thus becomes

$$D_{\mathrm{eff}}(\omega, v_{a,j}) = N\frac{\omega}{2\pi v_{a,j}^2} = \frac{\omega}{2\pi v_{a,j}^2}\frac{1}{d}, \tag{6}$$

where d is the interlayer spacing and $v_{a,j}$ is the polarization-specific Debye phonon group velocity in the basal plane [28, 29]. Therefore, realizing that under the Debye assumption the relationship between v, ω, and k simplifies such that

$$v = \frac{\partial\omega}{\partial k} = \frac{\omega}{k}, \tag{7}$$

thermal flux in graphite perpendicular to the interface reduces from the form of Eq. 2 to

$$q_{g,j,z} = \pi\sum_j \int_{\omega_{a,j}} \hbar\omega v_{z,j} D_{\mathrm{eff}}(\omega, v_{a,j}) f\, d\omega. \tag{8}$$

The subscript z denotes the orientation of the graphite relative to the interface and can take on two values, either a (basal planes perpendicular to the interface, transport along the basal planes), or c (basal planes parallel to the interface, transport perpendicular to the planes). Note that the density of states and cutoff frequency do not depend on the graphite orientation since the vibrational modes are assumed only to exist in the basal plane. Still, the propagation velocity does depend on the orientation. Three modes of vibration are still assumed within graphite (one longitudinal, two degenerate transverse). Phonon group velocities in the basal plane (a-axis) are taken as $v_{a,l} = 23,600$ m/s and $v_{a,t} = 15,900$ m/s [40]. A polarization-averaged group velocity is taken perpendicular to the planes, $v_c = 2,157$ m/s [44]. Assuming a planar lattice point density in graphite as $N_a = 1.9\times10^{19}$ m^{-2}, the a-axis cutoff frequency is defined as $\omega_{a,j} = v_{a,j}\sqrt{4\pi N_a}$. The thermal boundary conductance from a film to a graphite sub-

strate is then given by

$$h_{\mathrm{BD}}^{1\to g,z} = \frac{1}{4}\sum_{j}^{3}\int_{\omega_{\mathrm{D},j}} \hbar\omega v_{1,j} D_1(\omega, v_{1,j}) \frac{\partial f}{\partial T} \zeta^{1\to g,z}(\omega)\, d\omega, \quad (9)$$

where the metal properties are denoted by the sub- or superscript "1". In this work, a three-dimensional isotropic Debye density of states is used to describe the metal film, and $\omega_{\mathrm{D},j} = v_{1,j}\sqrt[3]{6\pi^2 N_a}$ [45]. Values for density, ρ_1, and velocities, $v_{1,j}$ are taken from Swartz and Pohl [30].

Following the theory from previous work developed to account for multiple phonon diffusive scattering events at solid-solid interfaces [42], Eq. 9 is reformulated to explicitly describe multi-phonon processes by utilizing a transmission coefficient that is separated into components. Here the analysis is limited to four and fewer phonon processes, as the contributions of higher order processes do not significantly contribute to h_{BD} at lower temperatures (below the Debye temperature of one or both materials comprising the interface) [42]. This approach enables the specific contributions to the transmission coefficient from the two-phonon elastic processes to be distinguished from contributions from the inelastic three- and four-phonons processes, yielding

$$h_{\mathrm{BD}}^{1\to g,z} = \frac{1}{4}\sum_{j}^{3}\int_{\omega_{\mathrm{D},j}} \hbar\omega v_{1,j} D_1(\omega, v_{1,j}) \frac{\partial f}{\partial T} \times \left(\zeta_{(2),j}^{1\to g,z}(\omega) + \zeta_{(3)}^{1\to g,z}(\omega) + \zeta_{(4)}^{1\to g,z}(\omega)\right) d\omega. \quad (10)$$

While this treatment of inelastic scattering may not be exact, it serves as a good first-approximation to the relative contribution of inelastic processes to thermal transport at interfaces. The elastic transmission coefficient (assuming two phonon scattering) is defined as outlined by [36] so that detailed balance on each phonon frequency yields

$$\hbar\omega D_1(\omega, v_{1,j}) f(\omega) \zeta_{(2),j}^{1\to g,z}(\omega) = \hbar\omega D_{\mathrm{eff}}(\omega, v_{a,j}) f(\omega) \zeta_{(2),j}^{g,z\to 1}(\omega), \quad (11)$$

which, assuming completely diffusive scattering ($\zeta^{1\to g,z} = 1 - \zeta^{g,z\to 1}$), yields a two phonon transmission coefficient of

$$\zeta_{(2),j}^{1\to g,z} = \frac{\dfrac{v_{z,j}}{v_{a,j}^2}\dfrac{1}{d}}{\dfrac{\omega}{\pi v_{1,j}^2} + \dfrac{v_{z,j}}{v_{a,j}^2}\dfrac{1}{d}}. \quad (12)$$

In the development of Eq. 12, the transmission coefficient is calculated on a per frequency, as well as per polarization, basis, which assumes not only completely elastic processes but also, in contrast to typical approaches of diffuse scattering, that a phonon of mode j can only couple with another phonon of the same mode. This ensures phonon number conservation for both the elastic as well as the higher order processes [40]. Although this abandons the pure definition of diffuse scattering (phonon loses memory and can scatter to any mode), in the Debye approximation, this assumption does not make a substantial difference in the overall result [28].

The determination of the three-phonon inelastic transmission probability begins with a balance similar to Eq. 11, only assuming two phonons of energy ω in the film will couple with a phonon of energy 2ω in the substrate, so that the balance equation becomes

$$2\hbar\omega v_{1,j} D_1(\omega, v_{1,j}) f(\omega) \zeta_{(3),j}^{1\to g,z}(1 - \zeta_{(2),j}^{1\to g,z}) = \hbar(2\omega) v_{z,j} D_{\mathrm{eff}}(2\omega, v_{a,j}) f(2\omega)(1 - \zeta_{(3),j}^{1\to g,z})\zeta_{(2),j}^{1\to g,z}, \quad (13)$$

when $0 < \omega \leq \frac{1}{2}\omega_{\mathrm{D},j}$ and

$$2\hbar\omega v_{1,j} D_1(\omega, v_{1,j}) f(\omega) \zeta_{(3),j}^{1\to g,z}(1 - \zeta_{(2),j}^{1\to g,z}) = \hbar(2\omega) v_{z,j} D_{\mathrm{eff}}(2\omega, v_{a,j}) f(2\omega) \zeta_{(3),j}^{g,z\to 1}, \quad (14)$$

when $\frac{1}{2}\omega_{\mathrm{D},j} < \omega \leq \omega_{\mathrm{D},j}$, where $f(2\omega) = [\exp(\hbar(2\omega)/k_{\mathrm{B}}T) - 1]^{-1}$. This gives a three phonon transmission coefficient, defined as

$$\zeta_{(3),j}^{1\to g,z} = \begin{cases} \dfrac{\dfrac{v_{z,j}}{v_{a,j}^2}\dfrac{1}{d} f(2\omega)\zeta_{(2),j}^{1\to g,z}}{\dfrac{\omega}{2\pi v_{a,j}^2} f(\omega)(1 - \zeta_{(2),j}^{1\to g,z}) + \dfrac{v_{z,j}}{v_{a,j}^2}\dfrac{1}{d} f(2\omega)\zeta_{(2),j}^{1\to g,z}}, \\ 0 < \omega \leq \frac{1}{2}\omega_{\mathrm{D},j} \\ \\ \dfrac{\dfrac{v_{z,j}}{v_{a,j}^2}\dfrac{1}{d} f(2\omega)}{\dfrac{\omega}{2\pi v_{a,j}^2} f(\omega)(1 - \zeta_{(2),j}^{1\to g,z}) + \dfrac{v_{z,j}}{v_{a,j}^2}\dfrac{1}{d} f(2\omega)}, \\ \frac{1}{2}\omega_{\mathrm{D},j} < \omega \leq \omega_{\mathrm{D},j} \end{cases}. \quad (15)$$

The development of the four-phonon process follows in similar fashion, but has been omitted from this work for the sake of brevity.

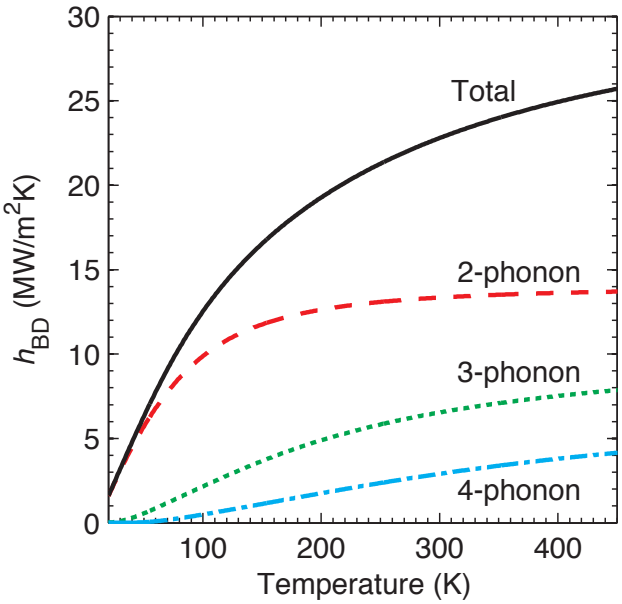

Figure 1. Individual contributions of two-, three-, and four-phonon processes for metal-to-c-axis h_{BD} at 300 K as a function of temperature.

The predicted temperature-dependent contributions to h_{BD} at Au-graphite interfaces from the two-phonon elastic process as well as the three- and four-phonon inelastic processes, assuming heat transport is perpendicular to the graphite structure (c-axis), are shown in Fig. 1. The total h_{BD} is the sum of the two-, three-, and four-phonon contributions. These results illustrate the fact that the contributions from inelastic processes become more significant as temperature increases. Table 1 lists the contributions of each process, as well as the total predicted for Au to c-axis graphite h_{BD} at 300 K. This model suggests that at room temperature, in excess of 40 % of the heat conducted across the Au-graphite interface is through inelastic channels.

MEASURING THERMAL BOUNDARY CONDUCTANCE

In order to investigate the effect of interfacial structure and chemistry on h_{BD}, three metal-on-graphite samples were prepared for experimental thermal characterization. The three samples consisted of thin Au films on 12 mm x 12 mm x 1 mm Grade 1 highly-ordered pyrolytic graphite substrates (HOPG) from Structure Probe Incorporated. Gold was chosen over other possible metals in order to reduce the number of variables affecting thermal transport across the interface. Previous work has shown that Au does not wet HOPG or other carbon-based substrates. As a result, the Au-HOPG surface interaction is characterized by weak van der Waals adhesion [23, 46, 47]. Thus, this choice of material system eliminated the variability of bonding reported when more reactive metals (e.g., Ti [22]) are deposited on HOPG.

Table 1. Individual contributions of two-, three-, and four-phonon processes for metal-to-c-axis h_{BD} at 300 K. All results in MW m^{-2} K^{-1}.

	2-phonon	3-phonon	4-phonon	Total
Au	13.3	6.5	2.9	22.8

Prior to metal deposition, each substrate underwent a different surface pretreatment to influence the interfacial structure and chemistry. The first substrate was cleaved using the "scotch tape method" to remove the first few layers of graphene, and no other pretreatment or cleaning method was used. The second substrate was cleaved in the same manner and subsequently ion cleaned. A 3 cm ion source, located 14 cm from the substrate, with a beam voltage of 300 V was used to surface etch the substrate, for a total exposure time of 7 minutes. As a means of comparison, exposing an SiO_2 wafer to these conditions removes approximately 5-10 nm of material from the surface and creates a disordered surface. The third substrate was again cleaved in the same manner and was subsequently electron cleaned. The conditions of the electron cleaning were the same as the ion cleaning, however, the beam voltage was turned off. It is presumed the electron heating from both the cathode filament and the neutralizer filament (which sits outside/at the end of the ion source) helps to remove surface water from the substrate. After all surface pretreatments, 50 nm of Au was deposited on the HOPG surface by DC sputtering. These three surface treatments should have a significant impact on the condition of Au-HOPG interface, as it has been demonstrated that contaminants and defects can lead to increased interaction between metals and HOPG [21, 22].

Thermal boundary conductance of each Au-HOPG interface was measured via TTR. Transient thermoreflectance [48–50] and its variations [51,52] are optical thermometry techniques that use pulsed laser systems to both heat and monitor the surface temperature of a metallic thin film. A schematic of the TTR system used in the Nanoscale Energy Transport Lab at the University of Virginia is shown in Fig. 2. The pulsed laser source was a Coherent Mira 900 oscillator pumped by $\sim$ 28% output from a Coherent Verdi V18, producing pulses on the order of several nJ per pulse at a repetition rate of 76 MHz. The output from the Mira 900 was then seeded into a Coherent RegA 9000 amplifier pumped by the remaining 72% output from the Verdi V18. The amplifier increases the pulse energy from several nJ to several μJ per pulse. The fundamental output of the amplifier was 1.55 eV at 250 kHz with $\sim$ 160 fs pulse widths.

A Newport 600 mm linear delay stage was used to delay the probe for a total of 4 ns temporal delay, while maintaining less that 2 μm of linear drift in the vertical and horizontal direction

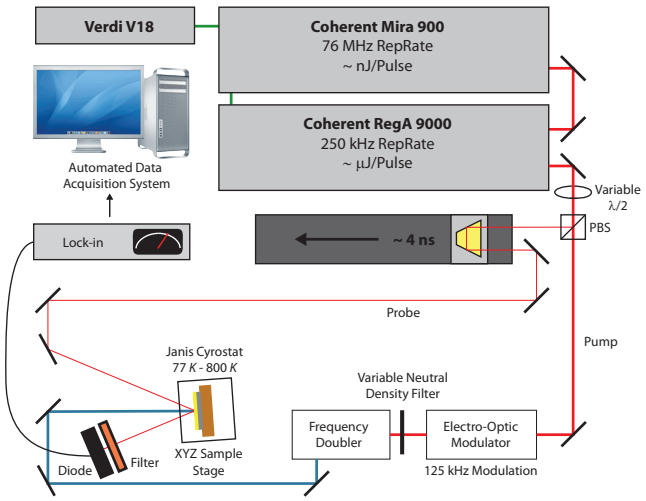

Figure 2. Schematic of the transient thermoreflectance system at the University of Virginia.

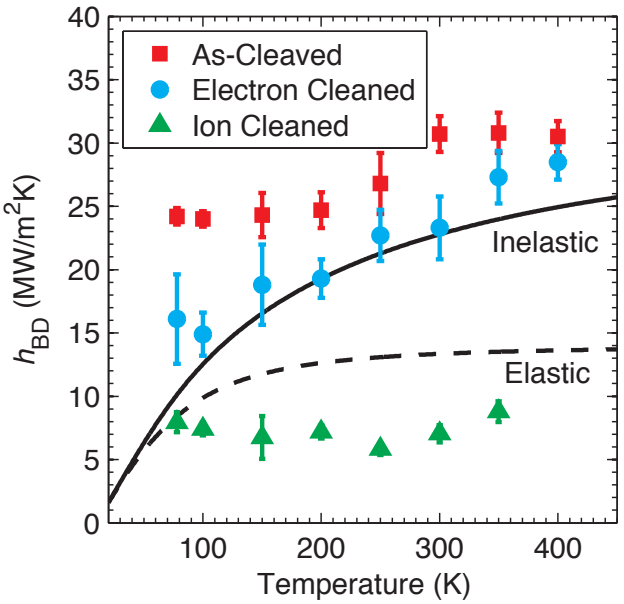

Figure 3. Temperature dependent thermal boundary conductance for Au/HOPG samples with various surface pre-treatments compared to theoretical elastic and inelastic models.

along the length of the stage. The pump beam was modulated using a Conoptics EOM at 125 kHz before being passed through a frequency doubling BBO crystal to improve signal-to-noise filtering. The pump and probe beam were focused down using objective lenses to a spot size of 236 μm $\pm$ 2 μm and 26 μm $\pm$0.6 μm respectively. For the data taken in this study, the incident pump fluence was set to $\sim$ 2 J/m^2.

Each of the prepared samples were thermally characterized via TTR at temperatures ranging from 78-400 K. In order to explicitly determine h_{BD}, the measured data are fit to a two-layer heat conduction model [12] and h_{BD} is adjusted such that the square of the difference between the raw data and the thermal model is minimized. An inverse parabolic interpolation technique is used during fitting to reduce the number of iterations required for the system to converge. The data of each scan are individually fit and a single "measured" value of h_{BD} is determined per scan; these fit values are subsequently averaged.

The temperature-dependent h_{BD} data is presented in Fig. 3. Each point in the figure represents the average of the ten measured values at that particular temperature. Error bars represent the standard deviation of the best fit h_{BD} for the 10 scans. As clearly evident in Fig. 3, different HOPG surface preparations drastically change the behavior of phonon transport across a Au-Graphite interface. The as-cleaved sample exhibited the highest values of h_{BD} across the entire temperature range, followed by the electron cleaned, and lastly, ion cleaned. The difference between measured h_{BD} for the as-cleaved and ion cleaned samples is in excess of 300 %, demonstrating how greatly surface preparation, and hence, the physical aspects of the interface, can impact interfacial thermal transport.

THEORETICAL AND EXPERIMENTAL COMPARISON

In addition to the experimental data, Fig. 3 also includes the elastic and inelastic predictions of phononic thermal transport at the Au-HOPG interface. From comparison of the experimental data and the predictive modeling, several important features are prominent. First, the electron-cleaned data demonstrates good agreement with the inelastic model. This can be explained in the sense that the electron cleaning effectively removes contaminants from the HOPG surface without inducing disorder. As a result, this interface nearly mimics the ideal interface assumed by models like the one presented above (it has been shown that freshly cleaved graphite in air has a surface roughness of less than 1 nm [53]). As a result, the model can accurately capture the behavior of phonon transport across the Au-HOPG interface. The presence of contaminants on the surface of the as-cleaved sample should lead to increased reactivity between Au and HOPG [21], suggesting increased adhesion strength, and hence, higher h_{BD} [24]. Lastly, the ion-cleaned HOPG substrate should be highly disordered as a result of the heavy ion bombardment. As has been shown by Hopkins *et al.* [13], increased atomic mixing and disorder at the interface has a detrimental effect on h_{BD}. While these trends can be inferred with confidence,

further structural characterization is still required.

CONCLUSION

Accurate predictions of h_{BD} utilizing the DMM vary depending on the the materials used, especially for highly acoustically mismatched and anisotropic materials, and the assumptions made. For the metal-graphite system, a combination of reduced dimensionality, highly anisotropic thermal properties, large acoustic mismatch, and poor interfacial adhesion require the extension of the traditional DMM proposed by Swartz and Pohl [30]. An anisotropic DMM was developed in order to account for the anisotropy of the substrate by means of a modified effective density of state, treating the substrate as a system of weakly coupled two-dimensional Debye subsystems. While this model works well at capturing the magnitude of an isotropic-anisotropic system, for the solid-graphite system the temperature trend is not fully captured. This is due to the fact that the large vibrational mismatch between the solid-graphite system allows for the possibility of additional thermal transport channels through inelastic phonon-phonon processes. To account for this additional process, the anisotropic DMM is extended further to account for the additional three- and four-phonon inelastic processes. With the consideration of both the anisotropic nature of the substrate and the high vibrational mismatch between the materials, the theoretical model and the experimental data match very well for the electron-cleaned sample, the sample most representative of the perfect theoretical interface. However, the model does not directly capture the results of the ion-cleaned and as-cleaved samples. This is due to the one factor that has not yet been considered, the interfacial chemistry between the metallic film and the graphite substrate. In order to have a model that captures both the vibrational and structural properties of interfacial transport, a rigorous study of interfacial bonding and structural effects is required.

ACKNOWLEDGMENT

The authors acknowledge financial support from the Office of Naval Research through a MURI grant (Grant No. N00014-07-1-0723) and the Air Force Office of Scientific Research (Grant No. FA9550-09-1-0245). J.C.D. is greatly appreciative for financial support from the National Science Foundation through the Graduate Research Fellowship Program. P.E.H. is grateful for funding from the LDRD program office through the Sandia National Laboratories Harry S. Truman Fellowship. Sandia National Laboratories is a multiprogram laboratory operated by Sandia Corporation, a wholly owned subsidiary of Lockheed-Martin Company, for the United States Department of Energy's National Nuclear Security Administration under Contract DE-AC04-94AL85000.

REFERENCES

[1] Saito, R., Dresselhaus, G., and Dresselhaus, M. S., 1998. *Physical properties of carbon nanotubes*. Imperial College Press, London.

[2] Choi, S. U. S., Zhang, Z. G., Yu, W., Lockwood, F. E., and Grulke, E. A., 2001. "Anomalous thermal conductivity enhancement in nanotube suspensions". *Applied Physics Letters,* **79**(14), pp. 2252–2254.

[3] Biercuk, M. J., Liaguno, M. C., Radosavljevic, M., Hyun, J. K., Johnson, A. T., and Fischer, J. E., 2002. "Carbon nanotube composites for thermal management". *Applied Physics Letters,* **80**(15), pp. 2767–2769.

[4] Xu, J., and Fisher, T. S., 2006. "Enhanced thermal contact conductance using carbon nanontube array interfaces". *IEEE Transactions on Components and Packaging Technologies,* **29**(2), pp. 261–267.

[5] Xu, J., and Fisher, T. S., 2006. "Enhancement of thermal interface materials with carbon nanotube arrays". *International Journal of Heat and Mass Transfer,* **49**, pp. 1658–1666.

[6] Zhang, K., Chai, Y., Yuen, M. M. F., Xiao, D. G. W., and Chan, P. C. H., 2008. "Carbon nanotbue thermal interface material for high-brightness light-emitting-diode cooling". *Nanotechnology,* **19**, p. 215706.

[7] Tong, T., Zhao, Y., Delzeit, L., Kashani, A., Meyyappan, M., and Majumdar, A., 2007. "Dense vertically aligned multiwalled carbon nanotube arrays as thermal interface materials". *IEEE Transactions on Components and Packaging Technologies,* **30**(1), pp. 92–100.

[8] Abel, P. B., Korenyi-Both, A. L., Honecy, F. S., and Pepper, S. V., 1994. "Study of copper on graphite with titanium or chromium bond layer". *Journal of Materials Research,* **9**(3), pp. 617–624.

[9] Datta, S. K., Tewari, S. N., Gatica, J. E., Shih, W., and Bentsen, L., 1999. "Copper-alloy impregnated carbon-carbon hybrid composites for electronic packaging applications". *Metallurgical and Materials Transactions A,* **30A**, pp. 175–181.

[10] Chen, G., 2005. *Nanoscale Energy Transport and Conversion: A Parallel Treatment of Electrons, Molecules, Phonons, and Photons*. Oxford University Press.

[11] Henry, A. S., and Chen, G., 2008. "Spectral phonon transport properties of silicon based on molecular dynamics simulations and lattice dynamics". *Journal of Computational and Theoretical Nanoscience,* **5**(2), pp. 141–152.

[12] Stevens, R. J., Smith, A. N., and Norris, P. M., 2005. "Measurement of thermal boundary conductance of a series of metal-dielectric interfaces by the transient thermoreflectance technique". *Journal of Heat Transfer,* **127**, pp. 315–322.

[13] Hopkins, P. E., Norris, P. M., Stevens, R. J., Beechem, T. E., and Graham, S., 2008. "Influence of interfacial mixing on

thermal boundary conductance across a chromium/silicon interface". *Journal of Heat Transfer,* **130**, p. 062402.

[14] Prasher, R., 2008. "Thermal boundary resistance and thermal conductivity of multiwalled carbon nanotubes". *Physical Review B,* **77**, p. 075424.

[15] Lyeo, H.-K., and Cahill, D. G., 2006. "Thermal conductance of interfaces between highly dissimilar materials". *Physical Review B,* **73**, p. 144301.

[16] Sinha, S. K., 1966. "Lattice dynamics of copper". *Physical Review,* **143**(2), Mar, pp. 422–433.

[17] Gilat, G., and Nicklow, R. M., 1966. "Normal vibrations in aluminum and derived thermodynamic properties". *Physical Review,* **143**(2), pp. 487–494.

[18] Nicklow, R., Wakabayashi, N., and Smith, H. G., 1972. "Lattice dynamics of pyrolytic graphite". *Physical Review B,* **5**(12), pp. 4951–4962.

[19] Stevens, R. J., Zhigilei, L. V., and Norris, P. M., 2007. "Effects of temperature and disorder on thermal boundary conductance at solid-solid interfaces: nonequilibrium molecular dynamics simulations". *International Journal of Heat and Mass Transfer,* **50**, pp. 3977–3989.

[20] Hopkins, P. E., and Stewart, D. A., 2009. "Contribution of d-band electrons to ballistic transport and scattering during electron-phonon nonequilibrium in nanoscale au films using an ab initio density of states". *Journal of Applied Physics,* **106**(5), p. 053512.

[21] Ma, Q., and Rosenberg, R. A., 1997. "Interaction of Al clusters with the (0001) surface of highly oriented pyrolytic graphite". *Surface Science,* **391**, pp. L1224 – L1229.

[22] Ma, Q., and Rosenberg, R. A., 1999. "Interaction of Ti with the (0001) surface of highly ordered pyrolitic graphite". *Physical Review B,* **60**(4), pp. 2827–2832.

[23] Dezellus, O., and Eustathopoulos, N., 1999. "The role of van der Waals interactions on wetting and adhesion in metal/carbon systems". *Scripta Materialia,* **40**(11), pp. 1283 – 1288.

[24] Prasher, R., 2009. "Acoustic mismatch model for thermal contact resistance of van der Waals contacts". *Applied Physics Letters,* **94**, p. 041905.

[25] Shenogin, S., Xue, L., Ozisik, R., Keblinski, P., and Cahill, D. G., 2004. "Role of thermal boundary resistance on the heat flow in carbon-nanotube composites". *Journal of Applied Physics,* **95**(12), pp. 8136–8144.

[26] Hu, M., Keblinski, P., Wang, J.-S., and Raravikar, N., 2008. "Interfacial thermal conductance between silicon and a vertical carbon nanotube". *Journal of Applied Physics,* **104**, p. 083503.

[27] Huxtable, S. T., Cahill, D. G., Shenogin, S., Xue, L., Ozisik, R., Barone, P., Usrey, M., Strano, M. S., Siddons, G., Shim, M., and Keblinski, P., 2003. "Interfacial heat flow in carbon nanotube suspensions". *Nat Mater,* **2**(11), 11, pp. 731–734.

[28] Duda, J. C., Smoyer, J. L., Norris, P. M., and Hopkins, P. E., 2009. "Extension of the diffuse mismatch model for thermal boundary conductance between isotropic and anisotropic materials". *Applied Physics Letters,* **95**, p. 031912.

[29] Duda, J. C., Hopkins, P. E., Beechem, T. E., Smoyer, J. L., and Norris, P. M., 2010. "Inelastic phonon interactions at solid-graphite interfaces". *Superlattices and Microstructures,* **47**, pp. 550–555.

[30] Swartz, E. T., and Pohl, R. O., 1989. "Thermal boundary resistance". *Reviews of Modern Physics,* **61**(3), pp. 605–667.

[31] Little, W. A., 1959. "The transport of heat between dissimilar solids at low temperatures". *Canadian Journal of Physics,* **37**(3), pp. 334–349.

[32] Stoner, R. J., and Maris, H. J., 1993. "Kapitza conductance and heat flow between solids at temperatures from 50 to 300 K". *Physical Review B,* **48**(22), pp. 16373–16387.

[33] Phelan, P. E., 1998. "Application of diffuse mismatch theory to the prediction of thermal boundary resistance in thin-film high-T_c superconductors". *Journal of Heat Transfer,* **120**, pp. 38–43.

[34] Hopkins, P. E., and Norris, P. M., 2007. "Effects of joint vibrational states on thermal boundary conductance". *Nanoscale and Microscale Thermophysical Engineering,* **11**(3), pp. 247–257.

[35] Norris, P. M., and Hopkins, P. E., 2009. "Examining interfacial diffuse phonon scattering through transient thermoreflectance measurements of thermal boundary resistance". *Journal of Heat Transfer,* **131**, p. 043207.

[36] Duda, J. C., Hopkins, P. E., Smoyer, J. L., Bauer, M. L., English, T. E., Saltonstall, C. B., and Norris, P. M., 2010. "On the assumption of detailed balance in prediction of diffusive transmission probability during interfacial transport". *Nanoscale and Microscale Thermophysical Engineering,* **14**(1), pp. 21–33.

[37] Duda, J. C., Beechem, T. E., Hopkins, P. E., Smoyer, J. L., English, T. E., and Norris, P. M., 2010. "The role of dispersion on phononic thermal boundary conductance". *Under Review*.

[38] Vincenti, W. G., and Kruger, C. H., 2002. *Introduction to Physical Gas Dynamics*. Krieger Publishing Company, Malabar, FL.

[39] Incropera, F. P., and DeWitt, D. P., 2002. *Fundamentals of Heat and Mass Transfer*, 5th ed. Wiley.

[40] Sun, K., Stroscio, M. A., and Dutta, M., 2009. "Graphite C-axis thermal conductivity". *Superlattices and Microstructures,* **45**, pp. 60–64.

[41] Hopkins, P. E., Norris, P. M., Phinney, L. M., Policastro, S. A., and Kelly, R. G., 2008. "Thermal conductivity in nanoporous gold films during electron-phonon nonequilibrium". *Journal of Nanomaterials*(418050).

[42] Hopkins, P. E., 2009. "Multiple phonon processes contributing to inelastic scattering during thermal boundary conductance at solid interfaces". *Journal of Applied Physics,* **106**(1), p. 013528.

[43] Kim, P., Shi, L., Majumdar, A., and McEuen, P. L., 2001. "Thermal transport measurements of individual multiwalled nanotubes". *Physical Review Letters,* **87**(21), p. 215502.

[44] Chen, Z., Jang, W., Bao, W., Lau, C. N., and Dames, C., 2009. "Thermal contact resistance between graphene and silicon dioxide". *Applied Physics Letters,* **95**(16), p. 161910.

[45] Kittel, C., 2005. *Introduction to Solid State Physics*, 8th ed. Wiley, Hoboken, New Jersey.

[46] Lopez-Salido, I., Lim, D. C., Dietsche, R., Bertram, N., and Kim, Y. D., 2006. "Electronic and geometric properties of Au nanoparticles on highly ordered pyrolytic graphite (HOPG) studied using x-ray photoelectron spectroscopy (XPS) and scanning tunneling microscopy (STM).". *Journal Physical Chemistry B,* **110**(3), pp. 1128–1136.

[47] Lee, J., Tanaka, T., Seo, K., Hirai, N., Lee, J.-G., and Mori, H., 2006. "Wetting of Au and Ag particles on monocrystalline graphite substrates". *Rare Metals,* **25**(5), pp. 469 – 472.

[48] Smith, A. N., Hostetler, J. L., and Norris, P. M., 2000. "Thermal boundary resistance measurements using a transient thermoreflectance technique". *Microscale Thermophysical Engineering,* **4**, pp. 51–60.

[49] Norris, P. M., Caffrey, A. P., Stevens, R. J., Klopf, J. M., McLeskey, J. T., and Smith, A. N., 2003. "Femtosecond pump-probe nondestructive examination of materials". *Review of Scientific Instruments,* **74**(1), pp. 400–406.

[50] Stevens, R. J., Smith, A. N., and Norris, P. M., 2006. "Signal analysis and characterization of experimental setup for the transient thermoreflectance technique". *Review of Scientific Instruments,* **77**, p. 084901.

[51] Cahill, D. G., Goodson, K., and Majumdar, A., 2002. "Thermometry and thermal transport in micro/nanoscale solid-state devices and structures". *Journal of Heat Transfer,* **124**, pp. 223–241.

[52] Cahill, D. G., Ford, W. K., Goodson, K. E., Mahan, G. D., Majumdar, A., Maris, H. J., Merlin, R., and Phillpot, S. R., 2003. "Nanoscale thermal transport". *Journal of Applied Physics,* **93**(2), pp. 793–818.

[53] Yang, S., Kooij, E. S., Poelsema, B., Lohse, D., and Zandvliet, H. J. W., 2008. "Correlation between geometry and nanobubble distribution on hopg surface". *EPL (Europhysics Letters),* **81**(6), p. 64006.